Dynamical effects and fluctuations of interaction-matrix elements for a ballistic quantum dot

L. Kaplan[1] and Y. Alhassid[2]

[1]*Department of Physics, Tulane University, New Orleans, Louisiana 70118, USA*

[2]*Center for Theoretical Physics, Sloane Physics Laboratory, Yale University, New Haven, Connecticut 06520, USA*

(Received 17 September 2009; published 23 May 2011)

We study matrix element fluctuations of the two-body screened Coulomb interaction and of the one-body surface charge potential in ballistic quantum dots, comparing behavior in actual chaotic billiards with analytic results previously obtained in a normalized random-wave model. We find that the matrix element variances in actual chaotic billiards typically exceed by a factor of 3 or 4 the predictions of the random-wave model, for dot sizes commonly used in experiments. We discuss dynamical effects that are responsible for this enhancement. These dynamical effects have an even more striking effect on the covariance, which changes sign when compared with random-wave predictions. In billiards that do not display hard chaos, an even larger enhancement of matrix element fluctuations is possible. These enhanced fluctuations have implications for peak spacing statistics and spectral scrambling for quantum dots in the Coulomb blockade regime.

DOI: 10.1103/PhysRevB.83.205312 PACS number(s): 73.23.Hk, 05.45.Mt, 73.63.Kv

I. INTRODUCTION

The statistical fluctuations of single-particle energies and wave functions of dots whose single-particle dynamics are chaotic can be well approximated by random matrix theory (RMT).[1] The mesoscopic fluctuations of the conductance through open dots that are strongly coupled to leads are then successfully described by RMT.[2] In the opposite limit of an almost-isolated dot, the charge is quantized and electron-electron interactions modify the mesoscopic fluctuations of the conductance. Many of the analytical tools used to describe such isolated interacting systems are discussed in the recent review by Ullmo.[3]

The randomness of the single-particle wave functions induces randomness into the interaction-matrix elements when the latter are expressed in the basis of the former. These matrix elements can be decomposed into an average and a fluctuating part. The average part of the interaction, when combined with the one-body kinetic energy and a confining potential, leads to the so-called universal Hamiltonian.[4,5] This universal Hamiltonian includes a charging energy term, an exchange interaction term that is proportional to the square of the total spin of the dot, and a Cooper-channel term (that is repulsive in a quantum dot and does not lead to the BCS instability). The fluctuating part of the interaction is suppressed by the Thouless conductance g_T, and in the limit $g_T \to \infty$, the dot is completely described by the universal Hamiltonian.

The charging energy term leads to charge quantization in a weakly coupled dot, and the conductance peak height distributions in such a dot were derived in Ref. 6 using the RMT statistics of the single-particle wave functions. Qualitative features of these peak height distributions as well as the parametric peak height correlation and the weak localization effect as a function of magnetic field[7,8] were confirmed in experiments.[9–11] Remaining discrepancies between theory and experiments regarding the temperature dependence of the width of the peak spacing distribution[12] and the peak height distributions[13] at low temperatures were explained by the inclusion of the exchange interaction term of the universal Hamiltonian.[14,15]

However, not all observed features of the peak spacing distribution can be explained by the exchange interaction alone. At low temperatures, the spacing is given by the second-order difference of the ground-state energy versus particle number. When only charging energy is present, the peak spacing distribution is expected to be bimodal because of spin effects. The exchange interaction (with realistic values of the exchange coupling constant in quantum dots) reduces this bimodality but cannot explain its *absence* in the experiments.[12,16–18] It is then necessary to consider the effect of the fluctuating part of the interaction beyond the universal Hamiltonian.

In the Hartree-Fock-Koopmans approach (or alternatively, using a perturbation theory in the screened Coulomb interaction), the peak spacing can be expressed in terms of certain interaction-matrix elements, and sufficiently large fluctuations of such matrix elements[19] might explain the absence of bimodality in the peak spacing distribution. It is therefore of interest to make accurate estimates of interaction-matrix element fluctuations in chaotic dots. These fluctuations are determined by single-particle wave function correlations. In a diffusive dot, such correlations are well understood and lead to an $O(\Delta/g_T)$ standard deviation in the interaction-matrix elements,[20,21] where Δ is the mean single-particle level spacing. Peak spacing fluctuations are also affected by a one-body surface charge potential induced by the accumulation of charge on the surface of the finite dot.[20] Matrix element fluctuations of the two-body interaction and one-body surface charge potential are also important for determining the statistical scrambling of the Hartree-Fock energy levels and wave functions as electrons are added to the dot.[22,23]

Wave-function correlations and interaction-matrix element fluctuations in a ballistic dot are less understood. In Ref. 24 we used a normalized random-wave model (see also Refs. 25–27) to obtain analytic expressions for interaction-matrix element variances and covariances in the regime of large Thouless conductance g_T for a ballistic two-dimensional (2D) dot. In such a dot, $g_T \sim kL$, where k is the Fermi wave number and L is the linear size of the dot (defined more precisely as the square root of the dot's area). Since $kL \sim \sqrt{N}$ where N is the number

of electrons in the dot, the $kL \gg 1$ limit in which the random-wave model is expected to hold is also the limit of many electrons in the dot. In the present paper, we systematically investigate matrix element fluctuations in real chaotic billiards, for $30 \leqslant kL \leqslant 70$, corresponding roughly to the parameter range relevant for experiments ($\sim$150–800 electrons in the dot). We show that fluctuations can be significantly enhanced due to dynamical effects, e.g., the variance may be enhanced by a factor of 3 or 4. Such enhancement can help in explaining the peak spacing distribution measured in the chaotic dots of Ref. 12.

On the other hand, the typical fluctuations of matrix elements in chaotic dots cannot explain the even broader peak spacing distributions in the experiment of Ref. 18. The small dots used in the latter experiment are probably nonchaotic (top gates were used), and this has motivated us to study fluctuations beyond the chaotic regime. We show that a large (i.e., order of magnitude) enhancement of the fluctuations is possible in nonchaotic billiards.

The outline of this paper is as follows. In Sec. II, we introduce the modified quarter-stadium billiard as a convenient model for investigating matrix element fluctuations in chaotic systems. In Sec. III we consider matrix elements of the two-body screened Coulomb interaction, and find strong enhancement of the fluctuations in comparison with random-wave predictions. Semiclassical corrections due to bounces from the dot's boundaries lead to an increase in the fluctuations, but do not correctly predict the scaling with kL in the experimentally relevant range. Insight into the underlying mechanism of fluctuation enhancement is obtained by studying a quantum map model, which is described in the Appendix. An important conclusion is that the expansion in $1/kL$, while asymptotically correct, can be problematic in quantifying matrix element fluctuation in the regime relevant to experiments.

In Sec. IV we extend our investigation to one-body matrix elements associated with the surface charge potential, and find similar fluctuation enhancements. Going beyond the variance, we examine the full matrix element distributions in Sec. V, and observe deviations from a Gaussian shape that are even stronger than the deviations found in the random-wave model.[24] In Sec. VI we study systems beyond the chaotic regime: billiards dominated by marginally stable bouncing-ball modes and billiards with mixed dynamics (i.e., partly regular and partly chaotic). Finally, in Sec. VII we briefly discuss some implications of the present work for the quantitative understanding of spectral scrambling and peak spacing statistics for quantum dots in the Coulomb blockade regime.

II. CHAOTIC BILLIARDS

Here we investigate how dynamical effects modify the fluctuations of interaction-matrix elements beyond our findings in the random-wave model.[24] Here and in Secs. III–V we treat exclusively geometries displaying hard chaos. (Systems with stable or marginally stable classical trajectories will be considered in Sec. VI.) To this end, we will use a chaotic system shown in Fig. 1—a modified quarter-stadium billiard geometry,[28] where the quarter circle has radius R and the straight edge of length aR has been replaced by a parabolic bump to eliminate bouncing-ball modes. Algebraically, the billiard shape is defined by

$$\begin{aligned} 0 \leqslant y/R \leqslant 1 - s\left(1 - \frac{x^2}{a^2R^2}\right), \quad 0 \leqslant x/R \leqslant a, \\ 0 \leqslant y/R \leqslant \sqrt{1-(x/R-a)^2}, \quad a \leqslant x/R \leqslant a+1, \end{aligned} \tag{1}$$

where s is a free dimensionless parameter.

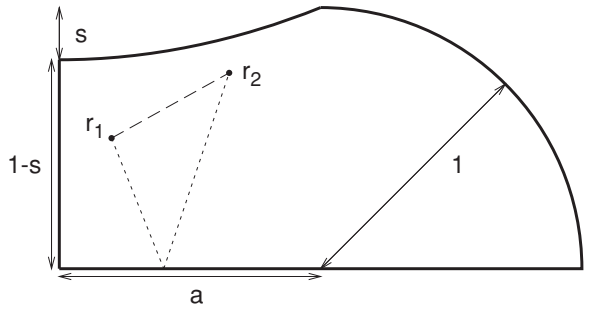

FIG. 1. A modified quarter-stadium geometry with parameters a and s is used to illustrate dynamical effects on matrix element fluctuations. In the figure, we set the quarter-circle radius $R = 1$. The random-wave contribution to the wave-function intensity correlator $C(\mathbf{r_1},\mathbf{r_2})$ is schematically indicated by a dashed line, and a typical dynamical contribution by a dotted line.

We use a quarter stadium instead of a full stadium shape in order to remove symmetry effects. This system has been verified numerically to be fully chaotic for the range of parameters used. Variation of the bump size s allows us to check the sensitivity of the results to details of the billiard geometry while maintaining the chaotic character of the classical dynamics. Furthermore, by varying the parameter a, we can control the degree of classical chaos. The degree of chaos can be characterized for example by the Lyapunov exponent λ, defined as the rate of divergence at long times of generic infinitesimally separated trajectories, $|\mathbf{r}(t) - \mathbf{r}'(t)| \sim |\mathbf{r} - \mathbf{r}'|e^{\lambda t}$ as $|\mathbf{r} - \mathbf{r}'| \to 0$ and then $t \to \infty$. For $a = 1.00$ and $0.1 \leqslant s \leqslant 0.2$, the exponent λ takes values $0.69 \leqslant \lambda T_B \leqslant 0.74$ (here $T_B = mL/\hbar k$ is a typical time scale associated with one bounce in the billiard). When $a = 0.25$, $0.55 \leqslant \lambda T_B \leqslant 0.56$ in the same range of s, indicating that the system is somewhat less chaotic for the smaller value of a. Other measures of the degree of chaoticity are possible and may be more relevant to the problem of matrix element fluctuations, as we will argue below. In particular, we may consider the rate λ_* of long-time decay of classical correlations, $\overline{f(q,p)f[q(t),p(t)]} - \overline{f(q,p)}^2 \sim e^{-\lambda_* t}$ as $t \to \infty$, where $f(q,p)$ is a typical function defined over the classical phase space and the average is over an energy hypersurface.[29] Numerically, we find $0.15 \leqslant \lambda_* T_B \leqslant 0.20$ for $a = 1$ and $0.095 \leqslant \lambda_* T_B \leqslant 0.13$ for $a = 0.25$, for the same range of bump sizes s as above, again indicating a less rapid approach to ergodicity in the $a = 0.25$ geometry.

An important consideration in the investigation of dynamical systems, as opposed to random-wave models, is the presence of boundary conditions. Boundary conditions lead to Friedel oscillations in the average wave-function intensity at distances $O(1/k)$ from a billiard boundary. The effect of such oscillations has recently been considered in

Refs. 25. The choice of boundary conditions, e.g., Neumann or Dirichlet, will also be seen to have significant effects on matrix element fluctuations, particularly on the fluctuations of one-body matrix elements.

Numerical wave functions for several values of the billiard parameters a, s and in various energy ranges have been calculated using a variation of the plane-wave method.[30] At each wave number k, a basis consisting of plane waves supplemented by a set of Y_0 Bessel functions centered a fraction of a wavelength outside the boundary is used; the size of the basis scales linearly with k. Singular value decomposition finds at each k the linear combination that minimizes the integrated squared deviation along the boundary from the selected boundary condition (Dirichlet or Neumann). Finally, minima of this deviation as a function of k indicate the correct eigenvalues of the system. Tests of the method include stability with respect to changes in the basis size and comparison of the resulting density of states with the Weyl formula.

Statistics are collected by averaging over an energy window. A straightforward estimate shows that such averaging is sufficient to give good results for matrix element variances, i.e., the ratio of signal to statistical noise grows with increasing kL. For all numerical results that follow, we use energy windows of constant momentum width $\Delta kL = 10$, e.g., the data point $kL = 30$ uses all wave functions within the window $25 \leqslant kL \leqslant 35$. The Weyl formula for the density of states in 2D implies that the number of wave functions in such a window grows linearly with kL.

III. TWO-BODY MATRIX ELEMENTS

A. Fluctuation of diagonal matrix elements $v_{\alpha\beta}$

We first study the variance of the diagonal two-body interaction-matrix elements $v_{\alpha\beta} \equiv v_{\alpha\beta;\alpha\beta}$, associated with a pair of electrons in distinct orbitals $\alpha \neq \beta$ interacting via the screened Coulomb force. Since the screening length of the Coulomb interaction in large 2D quantum dots is much smaller than the dot size, the interaction may be modeled as a contact interaction $v(\mathbf{r},\mathbf{r}') = \Delta V \delta(\mathbf{r}-\mathbf{r}')$, where $V = L^2$ is the dot's area, and the single-particle mean level spacing Δ serves to set the energy scale.[31,32] We then have

$$v_{\alpha\beta} = \Delta V \int_V d\mathbf{r} |\psi_\alpha(\mathbf{r})|^2 |\psi_\beta(\mathbf{r})|^2, \tag{2}$$

where the single-electron wave functions ψ obey the usual normalization condition $\int_V d\mathbf{r}|\psi(\mathbf{r})|^2 = 1$. To leading order in $1/g_T \sim 1/kL$, the variance is then given by[22,24]

$$\overline{\delta v_{\alpha\beta}^2} = \Delta^2 V^2 \int_V \int_V d\mathbf{r}\, d\mathbf{r}'\, C^2(\mathbf{r},\mathbf{r}') + O\left(\frac{\Delta^2}{(kL)^3}\right), \tag{3}$$

where

$$C(\mathbf{r},\mathbf{r}') = \overline{|\psi(\mathbf{r})|^2 |\psi(\mathbf{r}')|^2} - \overline{|\psi(\mathbf{r})|^2}\,\overline{|\psi(\mathbf{r}')|^2} \tag{4}$$

is the intensity correlator of a single-electron wave function at points $\mathbf{r}$ and $\mathbf{r}'$. Assuming $C(\mathbf{r},\mathbf{r}')$ is described by the normalized random-wave model (i.e., the single-electron wave functions are normalized as above with no boundary conditions), one obtains

$$\overline{\delta v_{\alpha\beta}^2} = \Delta^2 \frac{3}{\pi}\left(\frac{2}{\beta}\right)^2 \frac{\ln kL + b_g}{(kL)^2} + O\left(\frac{\Delta^2}{(kL)^3}\right), \tag{5}$$

where $\beta = 1$, 2 corresponds to the presence or absence of time-reversal invariance (i.e., the absence or presence of an external magnetic field), while b_g is a dimensionless coefficient that depends weakly on the dot geometry.[24] For a general dot shape, b_g is obtained by evaluating numerically the integral in Eq. (3), using the normalized random-wave intensity correlator $C(\mathbf{r},\mathbf{r}') = J_0^2(k|\mathbf{r}-\mathbf{r}'|) - \frac{1}{V}\int_V d\mathbf{r_a}\, J_0^2(k|\mathbf{r}-\mathbf{r_a}|) - \frac{1}{V}\int_V d\mathbf{r_a}\, J_0^2(k|\mathbf{r_a}-\mathbf{r}'|) + \frac{1}{V^2}\int_V\int_V d\mathbf{r_a}\, d\mathbf{r_b}\, J_0^2(k|\mathbf{r_a}-\mathbf{r_b}|)$.[24] For geometries considered in the present paper, b_g ranges between -0.07 and -0.10, and its variation is of negligible practical importance.

We now evaluate the variance of $v_{\alpha\beta}$ vs kL using "exact" (numerically evaluated) real wave functions in actual chaotic billiards. Typical results are shown in Fig. 2, where we note the large enhancement of the billiard results over the random-wave model (dotted line). To understand this enhancement, we compare the exact numerical results for $\overline{\delta v_{\alpha\beta}^2}$ with the first term on the right-hand side of Eq. (3), in which $C(\mathbf{r},\mathbf{r}')$ is taken to be the single-wave-function correlator $C_{\rm bill}(\mathbf{r},\mathbf{r}')$ calculated numerically for the appropriate billiard system. The discrepancy is immediately reduced to a ∼5%–10% level, which is comparable to the $O[(kL)^{-3}]$ higher-order correction expected and observed in the random-wave model. Thus, the large enhancement of $v_{\alpha\beta}$ fluctuations over the random-wave prediction is not due to higher-order terms in Eq. (3), but instead can be traced directly to a dynamical enhancement

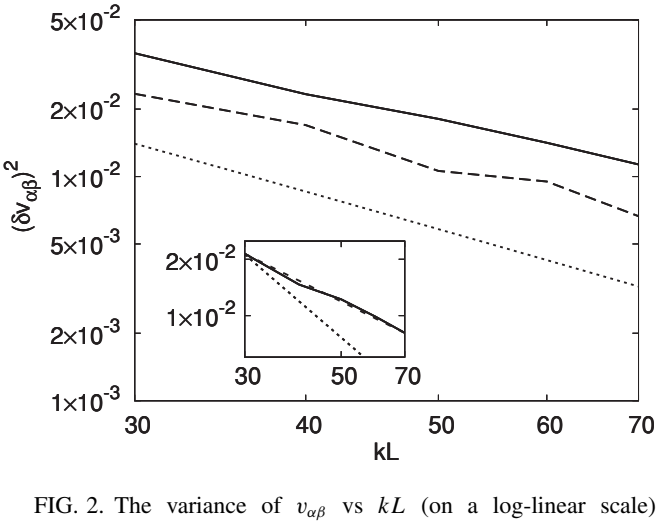

FIG. 2. The variance of $v_{\alpha\beta}$ vs kL (on a log-linear scale) for modified quarter-stadium billiards with Neumann boundary conditions. The solid line is for $a = 0.25$, while the dashed line is for $a = 1.00$. In both cases, the results are averaged over two values of the bump size: $s = 0.1$ and 0.2. Dotted line: Analytic random-wave prediction, Eq. (5), with $b_g = -0.10$. Inset: The numerical result for $a = 0.25$ with the leading logarithmic term of Eq. (5) subtracted (solid line) appears to fall off as $(kL)^{-1.15}$ (dashed line). The analytically expected subleading behavior $(kL)^{-2}$ is indicated by a dotted line for comparison.

in the intensity correlator $C_{\rm bill}(\mathbf{r},\mathbf{r}')$ over the random-wave correlator.

We next estimate the dynamical enhancement of the intensity correlator (as compared with a random-wave model) in a semiclassical approach. The random-wave correlator $C_{\rm rw}(\mathbf{r},\mathbf{r}')$ may be interpreted semiclassically as arising from straight-line free propagation[21] indicated by the dashed line in Fig. 1. As discussed by Hortikar and Srednicki[33] and more recently by Urbina and Richter,[34] additional contributions to the correlator can be associated with trajectories that bounce off the boundary n times on their way from $\mathbf{r}$ to $\mathbf{r}'$, such as the one indicated by a dotted line in Fig. 1. To find these contributions, we start from the dynamical correlator for wave-function amplitudes, which may be written as[26]

$$\overline{\psi^*(\mathbf{r})\psi(\mathbf{r}')} = \frac{\overline{G}^*(\mathbf{r},\mathbf{r}',E) - \overline{G}(\mathbf{r}',\mathbf{r},E)}{2\pi i\overline{\rho}(E)}. \tag{6}$$

Here $\overline{G}$ is the retarded Green's function $G(\mathbf{r},\mathbf{r}',E) = \sum_\alpha \frac{\psi_\alpha^*(\mathbf{r})\psi_\alpha(\mathbf{r}')}{E-E_\alpha+i\epsilon}$ smoothed on an energy scale much larger than the level spacing Δ and much smaller than the Thouless energy $kL\Delta$, and $\overline{\rho}(E)$ is the density of states $\rho(E) = \sum_\alpha \delta(E-E_\alpha)$, smoothed on the same energy scale. Using Eqs. (4) and (6), the dynamical intensity correlator is given by

$$C_{\rm bill}(\mathbf{r},\mathbf{r}') = \frac{2}{\beta}|\overline{G}(\mathbf{r}',\mathbf{r},E) - \overline{G}^*(\mathbf{r},\mathbf{r}',E)|^2/4\pi^2\overline{\rho}^2(E). \tag{7}$$

Semiclassically, i.e., to leading order in $1/kL$, the smooth density of states is given by the Weyl formula in 2D,

$$\overline{\rho}(E) = mL^2/2\pi\hbar^2, \tag{8}$$

while the Green's function to leading order in $1/kL$ is given by the Gutzwiller formula[35]

$$\overline{G}(\mathbf{r},\mathbf{r}',E) = \frac{1}{i\hbar(2\pi i\hbar)^{1/2}}\sum_j |D_j|^{1/2} e^{iS_j/\hbar - i\mu_j\pi/2}. \tag{9}$$

The sum in (9) is over classical trajectories j connecting $\mathbf{r}$ to $\mathbf{r}'$ at energy E, S_j is the action along the trajectory j, μ_j is the corresponding Maslov index, and D_j is a classical focusing factor that scales as m^2/pL_j (where p is the classical momentum and L_j is the trajectory length). For the straight-line trajectory, $|D_j| = m^2/p|\mathbf{r}-\mathbf{r}'|$. Inserting the semiclassical expressions (8) and (9) into Eq. (6), we obtain

$$\overline{\psi^*(\mathbf{r})\psi(\mathbf{r}')} = \frac{1}{V}[J_0(k|\mathbf{r}-\mathbf{r}'|) + h(\mathbf{r},\mathbf{r}')(kL)^{-1/2}], \tag{10}$$

where the Bessel function arises from the straight-line path, and $h(\mathbf{r},\mathbf{r}')$ is a sum over all other trajectories:

$$h(\mathbf{r},\mathbf{r}') = \sum_j{}' h_j(\mathbf{r},\mathbf{r}') = \sum_j{}' \left|\frac{2pLD_j}{\pi m^2}\right|^{\frac{1}{2}} \cos\left(\frac{S_j}{\hbar} - \frac{(2\mu_j+1)\pi}{4}\right). \tag{11}$$

For typical point pairs $(\mathbf{r},\mathbf{r}')$ separated by a distance of order L, the function $h(\mathbf{r},\mathbf{r}')$ is order unity in kL, and the contributions to the correlator from the straight-line path and from other paths are both $O[(kL)^{-1/2}]$. For pairs $(\mathbf{r},\mathbf{r}')$ separated by a bouncing path of length $L_j/L \leqslant \epsilon \ll 1$, $h(\mathbf{r},\mathbf{r}') \sim \epsilon^{-1/2}$. However, the fraction of such pairs is $O(\epsilon^3)$ and their contribution to the variance and other moments of matrix element distributions is negligible.

The intensity correlator in the semiclassical approximation becomes

$$C_{\rm sc}(\mathbf{r},\mathbf{r}') = \frac{1}{V^2}\frac{2}{\beta}\big[J_0^2(k|\mathbf{r}-\mathbf{r}'|) + h^2(\mathbf{r},\mathbf{r}')(kL)^{-1} + 2J_0(k|\mathbf{r}-\mathbf{r}'|)h(\mathbf{r},\mathbf{r}')(kL)^{-1/2}\big], \tag{12}$$

where the first (random-wave) term is associated with the straight-line path, and the remaining terms constitute semiclassical corrections.

Similarly to the random-wave correlator,[24,27,36] $C_{\rm sc}(\mathbf{r},\mathbf{r}')$ must be corrected to take into account individual wave-function normalization. [Since the numerator and denominator in (6) are both evaluated in a large-kL approximation, the resulting intensity correlator $C_{\rm sc}(\mathbf{r},\mathbf{r}')$ in general violates wave-function normalization at $O(1/kL)$.] In analogy with Refs. 24 and 36, we have, to leading order in $1/kL$,

$$\tilde{C}_{\rm sc}(\mathbf{r},\mathbf{r}') = C_{\rm sc}(\mathbf{r},\mathbf{r}') + \frac{1}{V^2}\int_V\int_V d\mathbf{r_a}\,d\mathbf{r_b}\,C_{\rm sc}(\mathbf{r_a},\mathbf{r_b}) - \frac{1}{V}\int_V d\mathbf{r_a}\,C_{\rm sc}(\mathbf{r},\mathbf{r_a}) - \frac{1}{V}\int_V d\mathbf{r_a}\,C_{\rm sc}(\mathbf{r_a},\mathbf{r}'). \tag{13}$$

Substituting $\tilde{C}_{\rm sc}$ for C in Eq. (3), we find

$$\overline{\delta v_{\alpha\beta}^2} = \Delta^2\frac{3}{\pi}\left(\frac{2}{\beta}\right)^2\frac{(\ln kL + b_g) + b_{\rm sc}}{(kL)^2} + O\left(\frac{\Delta^2}{(kL)^3}\right), \tag{14}$$

where $b_{\rm sc}$ is a classical constant that in practice must be determined numerically by performing the integral in Eq. (3). As noted above, the random-wave and semiclassical contributions to $C_{\rm sc}(\mathbf{r},\mathbf{r}')$ are of the same order except for $|\mathbf{r}-\mathbf{r}'| \ll L$; it is these short-distance pairs that result in a logarithmic enhancement of the random-wave term.

We may easily estimate the dependence of $b_{\rm sc}$ on the degree of chaoticity of the dynamical system by invoking a diagonal approximation, in which the intensity correlator $C_{\rm sc}(\mathbf{r},\mathbf{r}')$ of Eq. (12) is averaged over classically small regions surrounding $\mathbf{r}$ and $\mathbf{r}'$. Noting that Eq. (11) gives $h(\mathbf{r},\mathbf{r}')$ as a sum of oscillatory terms with quasirandom phases, such averaging leads to

$$C_{\rm sc}^{\rm dg}(\mathbf{r},\mathbf{r}') = \frac{1}{V^2}\frac{2}{\beta}\left[J_0^2(k|\mathbf{r}-\mathbf{r}'|) + \frac{1}{kL}\sum_j{}' h_j^2(\mathbf{r},\mathbf{r}')\right]. \tag{15}$$

We note from Eq. (11) that after averaging over wavelength-scale oscillations, $h_j^2(\mathbf{r},\mathbf{r}')/L = pD_j/\pi m^2$, which is proportional to the *classical* probability of traveling from a neighborhood of $\mathbf{r}$ to a neighborhood of $\mathbf{r}'$ via path j.[33,35] Thus, $\sum_j{}' h_j^2(\mathbf{r},\mathbf{r}')$ in Eq. (15) corresponds to the total classical probability of traveling from a neighborhood of $\mathbf{r}$ to a neighborhood of $\mathbf{r}'$ via paths j other than the straight-line path. Naively, the average semiclassical correction to the intensity correlator appears to increase as we include longer trajectories. However, let us organize the trajectories by number of bounces n or by time $t \sim nT_B$, where T_B is a typical time for one bounce in the billiard. Trajectories at times t that are

significantly longer than the classical correlation decay time λ_*^{-1} contribute only a constant, independent of $\mathbf{r}$ and $\mathbf{r}'$, to $C_{\rm sc}^{\rm dg}(\mathbf{r},\mathbf{r}')$. This is because a classical cloud of trajectories centered near $\mathbf{r}$ becomes approximately equidistributed over the entire billiard when $e^{\lambda_* t} \gg 1$, for any initial point $\mathbf{r}$. Such position-independent contributions to $C_{\rm sc}^{\rm dg}(\mathbf{r},\mathbf{r}')$ get subtracted off in the normalization procedure (13). Thus, the typical size of $C_{\rm sc}(\mathbf{r},\mathbf{r}')$ is determined by trajectories j having no more than $n_{\rm max} \approx (\lambda_* T_B)^{-1}$ bounces.

Furthermore, as a function of t, the number of classical trajectories typically grows as $e^{\lambda t}$, while the focusing factor for each trajectory j falls off as $|D_j| \sim e^{-\lambda t}$, where λ is the Lyapunov exponent defined earlier. Thus, all n-bounce trajectories combine to form a contribution to Eq. (15) whose order is roughly n independent for $n < n_{\rm max}$. Summing over n up to $n_{\rm max}$, where $n_{\rm max}$ is large, we find

$$C_{\rm sc}^{\rm dg}(\mathbf{r},\mathbf{r}') = \frac{1}{V^2}\frac{2}{\beta}\left[J_0^2(k|\mathbf{r}-\mathbf{r}'|) + O\left(\frac{n_{\rm max}}{kL}\right)\right]. \quad (16)$$

Going beyond the diagonal approximation is necessary to evaluate properly the integral in Eq. (3), but the scaling is unaffected [since the diagonal contribution $\sum_j' h_j^2$ consists of $O(e^{\lambda t})$ positive terms, whereas the off-diagonal contribution $\sum_{i\neq j}' h_i h_j$ consists of $O(e^{2\lambda t})$ entering with random signs]. Comparing Eqs. (3), (14), and (16), we obtain an estimate for the coefficient $b_{\rm sc}$ in Eq. (14) describing the semiclassical correction to the random-wave model,

$$b_{\rm sc} \sim n_{\rm max}^2 \sim (\lambda_* T_B)^{-2}. \quad (17)$$

This estimate confirms our intuition that semiclassical corrections to the random-wave approximation become increasingly important as we consider billiards with a very long ergodic time λ_*^{-1}.

Alternatively, the scaling (17) may be obtained by noting that when classical correlations persist on a time scale λ_*^{-1} that is much longer than the one-bounce time T_B, then the effective dimensionless Thouless conductance, which scales as the ratio of the Heisenberg time to the ergodic time, is reduced to $g_T \sim (T_B kL)/\lambda_*^{-1} \sim (\lambda_* T_B) kL$. Now a typical chaotic wave function $\psi_\alpha(\mathbf{r})$ may be written as a superposition of $O(g_T)$ nonergodic basis states $\eta_i(\mathbf{r})$. Since the correlator $\overline{\eta_i^*(\mathbf{r})\eta_i(\mathbf{r}')}$ for each nonergodic basis state η_i is of order V^{-1}, we easily see that $\overline{\psi_\alpha^*(\mathbf{r})\psi_\alpha(\mathbf{r}')}$ takes typical values of order $V^{-1} g_T^{-1/2}$. The wave-function intensity correlator $C_{\rm sc}(\mathbf{r},\mathbf{r}')$ scales as the square of the amplitude correlator, or as $V^{-2} g_T^{-1}$ for typical pairs $(\mathbf{r},\mathbf{r}')$, yielding a lower bound

$$\overline{\delta v_{\alpha\beta}^2} \sim \frac{\Delta^2}{g_T^2} \sim \frac{\Delta^2}{(\lambda_* T_B kL)^2} \quad (18)$$

for the integral (3), consistent with Eqs. (14) and (17).

For "generic" chaotic systems, the correlation decay time λ_*^{-1} is of the same order as the one-bounce time T_B, and the above asymptotic scaling arguments for $\lambda_* T_B \ll 1$ are not directly applicable. However, the first few bounces may be summed up numerically to obtain the semiclassical coefficient $b_{\rm sc}$. This coefficient may in practice be quite large even for generic chaotic systems (e.g., the modified stadium billiard) and grows as the system becomes less chaotic (and the time scale associated with nonuniversal behavior increases), in qualitative agreement with Eq. (17).

Qualitatively, the above discussion is consistent with our billiard results shown in Fig. 2, as fluctuations are observed to be consistently larger for the less chaotic $a = 0.25$ billiard, as compared with the $a = 1.00$ billiard. We note that both billiards are "generic," in the sense that they are not fine tuned to obtain an anomalously long time scale λ_*^{-1}.

However, a close look at the data suggests that the numerical results cannot be explained fully by semiclassical arguments, no matter how many bounces are included in the analysis. The semiclassical correction to the variance in Eq. (14) is manifestly $O[1/(kL)^2]$. However, the inset in Fig. 2 clearly shows that the dynamical contribution to the variance with kL is not consistent with Eq. (14) but instead appears to follow a much slower power law $\sim 1/(kL)^{-1.15}$. This may be seen also in Fig. 3 (solid line), where the enhancement over the random-wave prediction grows instead of diminishing with increasing kL. We also note in Fig. 3 the increase from $kL = 70$ to 140 in the enhancement of the double-diagonal matrix element variance $\overline{\delta v_{\alpha\alpha}^2}$ (dashed line), discussed below in Sec. III B. While this might be partly due to statistical noise, the data show clearly that wave-function fluctuations are not beginning to approach random-wave expectations even at $kL = 140$.

This anomalous behavior results from a combination of two related factors: the dynamical enhancement, discussed above, of the $b_{\rm sc}$ coefficient due to a finite correlation time scale λ_*^{-1} in an actual dynamical system, and the consequent saturation of the $1/(kL)^2$ behavior at moderate ($\lesssim$100) values of kL. As the classical system becomes less unstable and the correlation time λ_*^{-1} increases, $b_{\rm sc}$ also increases in accordance with Eq. (17), leading to greatly enhanced matrix element variance at very large values of kL. Because the variance is bounded above independent of kL, the $(kL)^{-2}$ growth in the

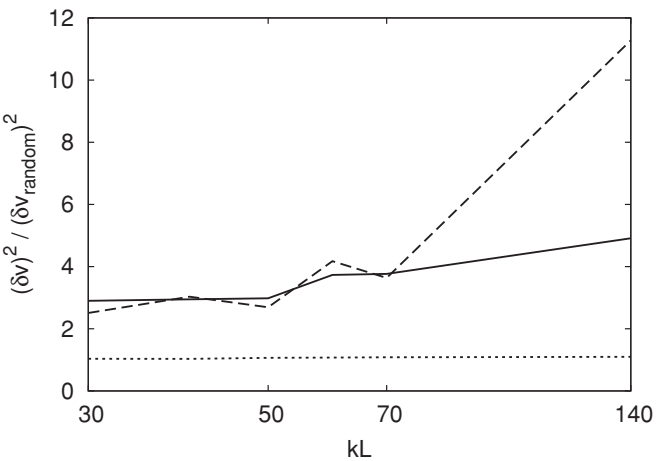

FIG. 3. The enhancement of the variance of $v_{\alpha\beta}$ (solid line), $v_{\alpha\alpha}$ (dashed line), and $v_{\alpha\beta\gamma\delta}$ (dotted line) over the corresponding random-wave predictions is shown for $a = 0.25$ billiards, at $kL = 30$, 40, 50, 60, 70, and 140. In each case, the data is averaged over bump sizes $s = 0.1$ and 0.2. See Sec. III B below for a discussion of $v_{\alpha\alpha}$ and $v_{\alpha\beta\gamma\delta}$. For $v_{\alpha\beta}$, the random-wave prediction is given by Eq. (5) with $b_g = -0.10$, and analogous expressions for $v_{\alpha\alpha}$ and $v_{\alpha\beta\gamma\delta}$ may be found in Ref. 24, with corresponding constants $b_g' = -2.25$ and $b_g'' = 0.90$, respectively.

variance necessarily breaks down for smaller values of kL. This small-kL saturation sets in at ever larger values of kL as the system becomes less unstable and λ_*^{-1} becomes larger.

Alternatively, one may note that the natural expansion parameter for interaction-matrix element fluctuations in a dynamical system is not $(kL)^{-1}$ but rather the inverse Thouless conductance $g_T^{-1} \sim (\lambda_* T_B kL)^{-1}$, and the semiclassical contribution with prefactor $b_{\rm sc}$ in Eq. (14) is the leading $O(g_T^{-2})$ effect in such an expansion. Terms of third and higher order in g_T^{-1}, although formally subleading and not included in a semiclassical calculation, become quantitatively as large as the leading $O(g_T^{-2})$ term when g_T falls below some characteristic value. This is a signature of the breakdown of the semiclassical expansion (14) in the calculation of interaction-matrix element fluctuations. Furthermore, if one considers chaotic billiards with a long correlation decay time λ_*^{-1}, the importance of formally subleading terms in the g_T^{-1} expansion, and thus the breakdown of the semiclassical expansion, will extend to quite large values of kL. These results suggest that interaction-matrix element statistics are particularly sensitive to long-range wave-function correlations that go beyond the semiclassical approximation. We remark that there is no conflict here with the well-known fact that semiclassical approximations may work quite well in the evaluation of other types of statistical quantities, even in the same billiard systems as the ones being considered here and in the same kL regime.

The above assertions are explicitly confirmed for a quantum map model, described in detail in the Appendix, which has scaling behavior analogous to that of a 2D billiard, with the number of states $N = 2\pi/\hbar$ playing the role of semiclassical parameter $kL = pL/\hbar$ in the billiard.[37,38] As in the billiard, a free parameter in the definition of the map allows for control of the classical correlation decay time λ_*^{-1}. A key difference between the 2D billiard and the map model is that the map lacks a logarithmic random wave contribution to the variance. We see in Fig. 4 that the expected N^{-2} behavior of the variance is observed at sufficiently large N, for all three families of quantum maps considered. Furthermore, the prefactor multiplying N^{-2} in each case agrees with that obtained from a semiclassical calculation, and as expected this prefactor grows with increasing classical correlation time λ_*^{-1} (corresponding to a decrease in the chaoticity of the system). We also see in Fig. 4 that even for a "typical" chaotic system (i.e., $\lambda_* T_B \sim 1$), strong deviations from the $1/N^2$ law appear already below $N \approx 80$. Such deviations extend to even larger N for chaotic systems with slower classical correlation decay. Based on results shown in Fig. 4 and the scaling $N \sim kL$, it is reasonably safe to conclude that the large-N or large-kL expansion will be valid for $kL \sim 1000$, corresponding to $\sim 10^5$ electrons in the dot. At the same time we see that this expansion, though theoretically appealing and asymptotically correct, is problematic in describing the quantitative behavior of interaction-matrix element fluctuations for real chaotic systems in the physically interesting energy range $kL < 100$.

The above numerical calculations were all performed in the presence of time-reversal symmetry ($\beta = 1$). From Eq. (14) we see that when time-reversal symmetry is broken ($\beta = 2$), both the random-wave contribution to the matrix element variance

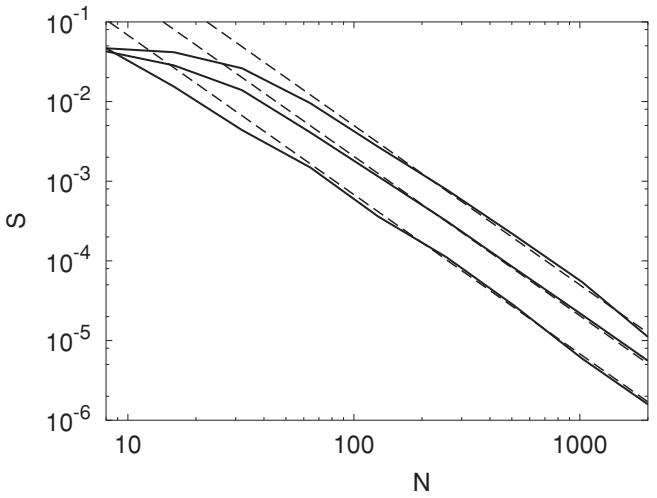

FIG. 4. The two-body matrix element variance S for a quantum map, Eq. (A6) in the Appendix, as a function of the Hilbert space dimension N. From top to bottom, the three solid lines represent data for dominant orbit stability exponent $\lambda_0 = 0.25, 0.50, 1.00$. The three dashed lines indicate the asymptotic $1/N^2$ behavior for each case in the semiclassical regime of large N, where the theoretical prefactors are obtained from the classical dynamics.

(the term proportional to $\ln kL + b_g$) and the semiclassical contribution (the term proportional to $b_{\rm sc}$) are suppressed by the same factor of 4. Thus, the dynamical enhancement factor for a given dot geometry is necessarily β independent in the semiclassical limit $kL \gg 1$. However, the saturation effect, which tends to suppress the enhancement as kL is reduced, will be less important when $\beta = 2$, since the variance is smaller in this case. Thus, at any finite value of kL, the dynamical enhancement in the variance over the random-wave model will be greater when time-reversal symmetry is broken, and one may expect enhancements somewhat larger than those shown in Fig. 3. This result has been confirmed in the quantum map model.

B. Fluctuation of $v_{\alpha\alpha}$ and $v_{\alpha\beta\gamma\delta}$

We have similarly studied the variance $\overline{\delta v_{\alpha\alpha}^2}$ of double-diagonal interaction-matrix elements and the variance $\overline{\delta v_{\alpha\beta\gamma\delta}^2}$ of off-diagonal interaction-matrix elements for actual chaotic billiards. Once again, the random-wave predictions[24] are used as the baseline for comparison. In Fig. 3, we show the enhancement factor for these matrix element variances, together with the corresponding data for $\overline{\delta v_{\alpha\beta}^2}$ discussed previously.

In the range $30 \leqslant kL \leqslant 70$ most relevant to experiment, we observe an enhancement in $\overline{\delta v_{\alpha\alpha}^2}$ over the random-wave prediction that is similar to the enhancement in $\overline{\delta v_{\alpha\beta}^2}$ in the same energy range. In both cases, the enhancement factor continues to grow, instead of approaching unity, at increasing kL. This latter fact strongly suggests that even at $kL = 140$, we are still far from the asymptotic regime of large g_T, where matrix element fluctuations would be adequately described by a random-wave picture supplemented by semiclassical corrections. The enhancement at large kL is particularly

dramatic in the case of $\overline{\delta v_{\alpha\alpha}^2}$ fluctuations. On the other hand, the variance of off-diagonal matrix elements $v_{\alpha\beta\gamma\delta}$ is enhanced over the random-wave prediction by at most 10% over the entire energy range considered. This is consistent with the reasonable expectation that dynamical effects lead to particularly strong deviations from random-wave behavior in a modest fraction of the total set of single-particle states, such as those associated with particularly strong scarring on unstable periodic orbits.[39] Such deviations lead to a significant tail in the $v_{\alpha\alpha}$ distribution, but have a minimal effect on the distribution of off-diagonal matrix elements, since it is unlikely for all four wave functions ψ_α, ψ_β ψ_γ, and ψ_δ to be strongly scarred or antiscarred on the same orbit.

Indeed, inspection of wave functions ψ_α associated with anomalously large double-diagonal matrix elements $v_{\alpha\alpha}$ shows that these wave functions have disproportionately high intensity on average near the dominant horizontal bounce periodic orbit, which follows the lower edge of the billiard in Fig. 1. We note, however, that asymptotic scar theory in the $kL \to \infty$ limit predicts $O[1/(kL)]$ corrections to the intensity correlation function in position space and only in a region of size $O[1/(kL)^{1/2}]$ surrounding a periodic orbit. Comparing with the integral expression (3) for the variance, we see that periodic orbits asymptotically contribute to the variance only at order $1/(kL)^3$, compared to the $O[1/(kL)^2]$ semiclassical effect associated with generic (nonperiodic) classical trajectories (14). Thus, the relative importance of periodic orbit effects on matrix element fluctuations is a finite-kL (or finite-$\hbar$) phenomenon, which cannot explain the quantitative scaling behavior of the variance with kL, and which is expected to become irrelevant in the asymptotic $kL \to \infty$ limit.

C. Matrix element covariance $\overline{\delta v_{\alpha\beta}\delta v_{\alpha\gamma}}$

The normalized random-wave model has been shown to produce a covariance $\overline{\delta v_{\alpha\beta}\delta v_{\alpha\gamma}}$ that is always negative, has size $\sim \Delta^2 \ln kL/(kL)^3$ for small $\omega = E_\beta - E_\gamma$, and falls off as $(\omega/E_T)^{-2} \sim (\delta kL)^{-2}$ for $\omega \gg E_T$, where E_T is the ballistic Thouless energy.[24] However, in a diffusive dot, the same matrix element covariance is found to be a *positive* constant $\propto \Delta^2/g_T^3$ (where g_T is the diffusive Thouless conductance) for energy separations ω much smaller than the diffusive Thouless energy E_c. This diffusive covariance falls off for $\omega \gg E_c$ but remains positive as long as $\omega \ll \hbar/\tau$, where τ is the mean free time.[22] An interesting issue is then the sign of the covariance in an actual chaotic system.

First we note the sum rule,[24]

$$\sum_{\beta\neq\gamma} \overline{\delta v_{\alpha\beta}\delta v_{\alpha\gamma}} = -\sum_{\beta} \overline{(\delta v_{\alpha\beta})^2}. \tag{19}$$

This sum rule is quite general and holds for either a ballistic or a diffusive dot as long as a completeness relation is satisfied within an energy window in which the states β and γ reside. The average covariance must therefore be negative when averaged over all states β and γ within such an energy window. The size of the energy window in each case must be at least of size $\hbar$ multiplied by the inverse time scale of first recurrences. In a ballistic system this implies an energy window of size at least $E_0 = \hbar/T_B$, where T_B is the one-bounce time. In a diffusive system, the completeness relation requires energy scales larger than $E_0 = \hbar/\tau$, where τ is the mean free time, and thus the positive sign of the diffusive covariance at energy separations $\omega \ll \hbar/\tau$ does not contradict the sum rule (19).

In actual chaotic billiards, it is in principle possible to find positive covariance at energy scales $\omega \ll E_0$, as long as the covariance is sufficiently negative for $\omega \sim E_0$ to produce a negative average covariance over the full energy window that is consistent with the sum rule (19). Such positive covariance can result from scars since ψ_β and ψ_γ will typically be scarred or antiscarred along the same orbits when $\omega = E_\beta - E_\gamma$ is small. The scar contribution to the covariance for small ω is $O[1/(kL)^3]$ (i.e., of the same order as the scar contribution to the variance) and is formally subleading compared with the negative $O[\ln kL/(kL)^3]$ random-wave contribution. However, within the range of kL values relevant to experiments, the scar contribution can dominate and lead to a positive covariance for nearby single-particle wave functions.

Unfortunately, it is not practical to calculate the matrix element covariance in a real billiard, since the number of wave functions that can be averaged over is not sufficient to obtain a signal larger than the statistical noise. We instead obtain good statistics for the covariance in a ballistic discrete map model, introduced previously in the discussion of the variance, and described in detail in the Appendix. In such discrete maps, the matrix element variance or covariance contains no logarithmic terms. For generic chaotic ballistic systems (i.e., Lyapunov time of the same order as the one-step time), we find that the covariance is $O(N^{-3}) \sim O[(kL)^{-3}]$ and positive for $\omega \ll E_0 = \hbar/T_B$, but becomes negative at $\omega \sim E_0$, in contrast with the random-wave prediction of an always negative covariance. A typical example for $N = 128$ is shown in Fig. 5. Here discreteness of time implies energy periodicity with period $2\pi E_0 = 2\pi\hbar/T_B$, and thus a maximum energy separation $\omega = \pi E_0$. In Fig. 5, the dotted line indicates the negative average covariance over the entire energy window

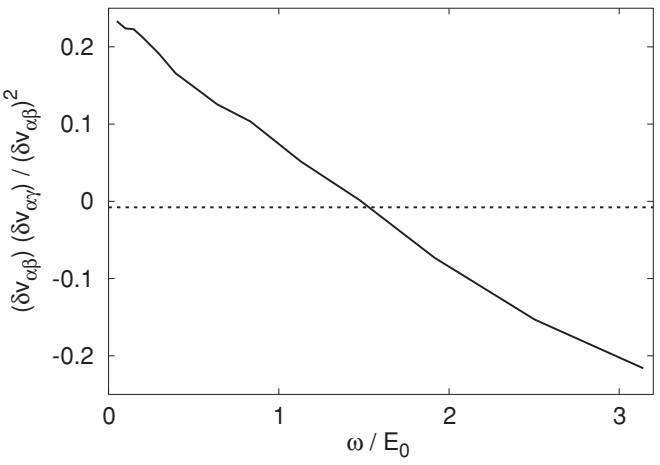

FIG. 5. The covariance $\overline{\delta v_{\alpha\beta}\delta v_{\alpha\gamma}}$ is computed as a function of energy separation $\omega = E_\beta - E_\gamma$ for an ensemble of ballistic discrete-time maps, described in the Appendix, Eqs. (A9) and (A10). Here $E_0 = \hbar/T_B$, where T_B is the one-bounce time. The system size N is 128, and $A = 0$. The dotted line indicates the negative average covariance implied by the sum rule (19).

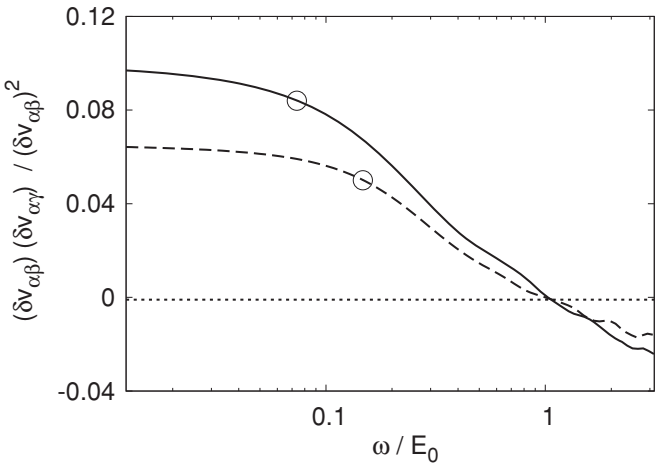

FIG. 6. The covariance $\overline{\delta v_{\alpha\beta}\delta v_{\alpha\gamma}}$ is computed as a function of energy separation $\omega = E_\beta - E_\gamma$ for an ensemble of diffusive discrete-time maps on a 32×32 lattice (Ref. 40). The solid curve corresponds to Thouless conductance $g_T = 12$ ($E_c/E_0 = 0.074$) and the dashed curve corresponds to $g_T = 24$ ($E_c/E_0 = 0.147$). Here $E_0 = \hbar/\tau$, where τ is the mean free time. The value $\omega = E_c$, below which the covariance is expected to approach a constant positive value, is indicated by a circle in each case. The dotted line indicates the negative average covariance implied by the sum rule (19).

of size $2\pi E_0$, as required by the sum rule (19). We note that due to partial cancellation between positive covariance at small energy separations and negative covariance at larger separations, the average covariance is noticeably smaller than the "typical" value, although both scale as $O(N^{-3})$.

It is interesting to compare with the covariance in an ensemble of two-dimensional diffusive discrete maps.[40] Typical data is shown in Fig. 6 for an ensemble of diffusive maps on a 32×32 lattice, with Thouless conductance $g_T = 12$ (solid curve) and $g_T = 24$ (dashed curve). The theory predicts a variance scaling as $1/g_T^2$ and a covariance scaling as $1/g_T^3$, so $\overline{\delta v_{\alpha\beta}\delta v_{\alpha\gamma}}/\overline{\delta v_{\alpha\beta}^2}$ should scale as $1/g_T$ in the $g_T \to \infty$ limit. Just as in the ballistic case, the covariance is positive for small separations ω and becomes negative when $\omega \sim E_0$. The average covariance over a maximal energy window of size $2\pi E_0$ is again negative, as predicted by the sum rule (19) and indicated by a dotted line.

IV. ONE-BODY MATRIX ELEMENTS

When an electron is added to the finite dot, charge accumulates on the surface and its effect can be described by a one-body potential energy $\mathcal{V}(\mathbf{r})$, which diverges at the boundary of the dot. For comparison with the random-wave predictions, we use the schematic approximation

$$\mathcal{V}(\vec{r}) \sim \left(\min_{\vec{R}\in\mathcal{C}} |\vec{r} - \vec{R}| \right)^{-\frac{1}{2}}, \tag{20}$$

which was shown in Ref. 24 to correctly capture the effect of the one-body potential energy in the random wave model. Here $\mathcal{C}$ is the boundary of the billiard, and the schematic potential (20) is normalized to have the same average as the true one-body potential.[24]

The diagonal matrix elements of $\mathcal{V}(\mathbf{r})$ are given by $v_\alpha \equiv \mathcal{V}_{\alpha\alpha} = \int_V d\mathbf{r}|\psi_\alpha(\mathbf{r})|^2\mathcal{V}(\mathbf{r})$, and the variance of these one-body matrix elements may be computed as

$$\overline{\delta v_\alpha^2} = \int_V \int_V d\mathbf{r}\, d\mathbf{r}'\, \mathcal{V}(\mathbf{r})C(\mathbf{r},\mathbf{r}')\mathcal{V}(\mathbf{r}'). \tag{21}$$

Dynamical enhancement of one-body matrix element fluctuations may be studied similarly to the analysis of two-body matrix element fluctuations presented in Sec. III. The leading semiclassical contribution to the variance is obtained by substituting the normalized semiclassical intensity correlator $C_{\rm sc}^{\rm dg}$ [see Eq. (16)] for $C(\mathbf{r},\mathbf{r}')$ in Eq. (21). We immediately obtain

$$\overline{\delta v_\alpha^2} = \frac{c_g + c_{\rm sc}}{\beta}\frac{\Delta^2}{kL} + O\left(\frac{\Delta^2}{(kL)^2}\right), \tag{22}$$

where c_g is a geometry-dependent dimensionless coefficient arising already in the random-wave model,[24] while $c_{\rm sc} \sim (\lambda_* T_B)^{-1}$ is associated with the classical dynamics. We note that the asymptotic power-law behavior of the variance is unchanged from the random wave model, and the variance is enhanced only by a kL-independent constant.

Numerical data for $\overline{\delta v_\alpha^2}$ in modified quarter-stadium billiards is presented in Fig. 7, and compared with random-wave results. The ratio of the actual variance to the random-wave prediction is shown in Fig. 8. Clearly this ratio is not constant but rather grows with kL (as was also the case with the $v_{\alpha\beta}$ variance). Assuming that semiclassical expressions are applicable in the asymptotic large-kL regime, the results of Fig. 8 indicate once again that at $kL \approx 70$ this regime is still far from being reached. The same can be observed by comparing data for Neumann and Dirichlet boundary conditions in Fig. 7. Since Dirichlet wave functions decay to zero at distances less than $1/k$ from a boundary, where the surface potential is especially strong, we expect larger matrix element fluctuations for the Neumann boundary condition

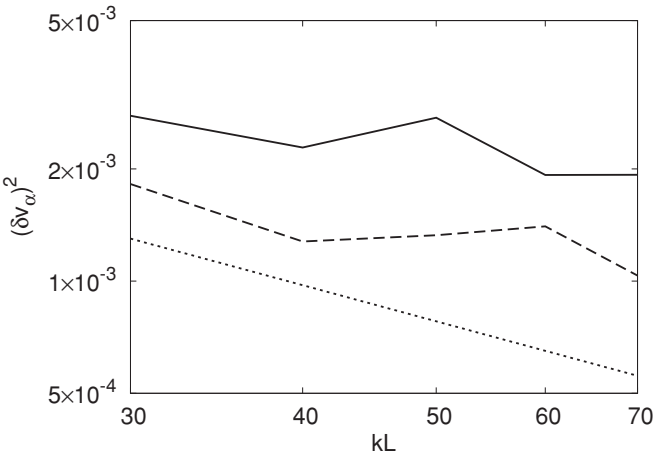

FIG. 7. The variance of the one-body diagonal matrix element v_α for modified quarter-stadium billiards ($a = 0.25$; averaged over $s = 0.1$ and 0.2) is plotted as a function of semiclassical parameter kL. Solid line: Neumann boundary conditions. Dashed line: Dirichlet boundary conditions on curved boundaries, and Neumann boundary conditions elsewhere. Dotted line: Analytic prediction for the random-wave model [given by Eq. (22), including only the c_g term].

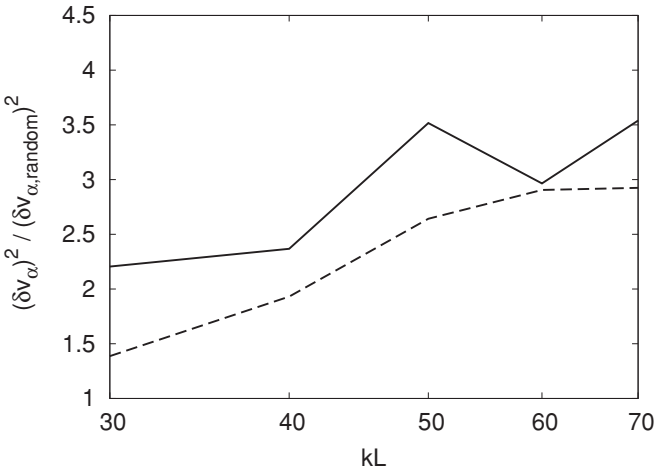

FIG. 8. Enhancement factor of the v_α variance over the random-wave prediction is plotted for modified quarter-stadium billiards with Neumann boundary conditions, averaged over $s = 0.1$ and 0.2. Solid line: $a = 0.25$; dashed line: $a = 1.00$.

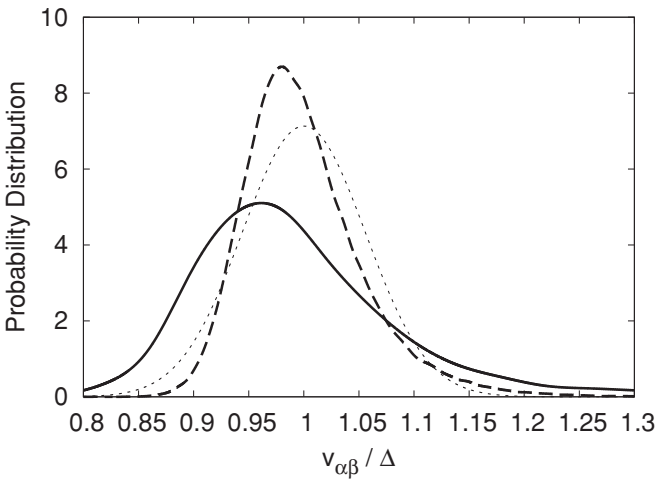

FIG. 9. The distribution of diagonal interaction-matrix elements $v_{\alpha\beta}$ is shown for real random waves in a disk (Ref. 24) (dashed curve) and for actual eigenstates in a modified quarter-stadium billiard geometry with Neumann boundary conditions (solid curve) at $kL = 70$. A Gaussian distribution with the same mean and variance as the random-wave distribution is shown as a dotted curve for comparison.

data, qualitatively consistent with the results in the figure. However, the fraction of points $\mathbf{r}$ so close to the boundary is $O(1/kL)$, while the surface potential $\mathcal{V}(\mathbf{r})$ is only enhanced by $O[(kL)^{1/2}]$ there, so the boundary condition effect is formally subleading. Nevertheless, we clearly see from the figure that in the energy range of experimental interest, the boundary condition effect is of size comparable both to the dynamical enhancement and to the baseline random-wave prediction for the variance.

V. MATRIX ELEMENT DISTRIBUTIONS

Just as was done previously for the random-wave model,[24] we can go beyond the variance to investigate higher moments of the matrix element distribution for actual chaotic systems. A typical distribution for diagonal two-body matrix elements $v_{\alpha\beta}$ in a modified quarter-stadium billiard with $a = 0.25$ and $s = 0.1$ is shown in Fig. 9. Since the approach to Gaussian behavior is already very slow in the case of random waves, it is not surprising to find even stronger deviations from a Gaussian shape for matrix elements in real chaotic systems at the same energies. Thus, for modified quarter-stadium billiards with $a = 1$, the skewness γ_1 of the $v_{\alpha\beta}$ distribution *grows* from 1.95 at $kL = 70$ to 2.72 at $kL = 140$, while the skewness for the same geometry in the random-wave model drops slightly from 1.21 to 1.09. Similarly, the excess kurtosis γ_2 increases from 8.3 at $kL = 70$ to 20.9 at $kL = 140$, while dropping from 3.7 to 3.3 in the random-wave model. Similar behavior is obtained for other matrix elements. Clearly, the distribution tails are very long, and the assumption of Gaussian matrix element distributions is even less justified for real chaotic systems than it was in the random-wave model.

VI. BEYOND THE CHAOTIC REGIME

In this section we consider fluctuations of matrix elements in systems that are not fully chaotic. Here no universal behavior is expected but we shall see that in such systems the variance can be enhanced much more than in fully chaotic systems.[32]

We use the modified quarter-stadium billiard [see Eq. (1)] with $s = 0$ or $a < 0$. The choice $s = 0$ corresponds to the original Bunimovich stadium, whose quantum fluctuation properties are dominated by the marginally stable bouncing-ball modes, while $a < 0$ corresponds to a lemon billiard, which has a classically mixed, or soft chaotic, phase space.

A. Two-body matrix elements

1. *Fluctuation of diagonal matrix elements $v_{\alpha\beta}$*

In contrast with the $\ln kL/(kL)^2$ falloff in the $v_{\alpha\beta}$ variance predicted for fully chaotic dynamics by Eq. (14), in the case of regular or mixed dynamics we expect kL-independent matrix element fluctuations of order unity. To see this explicitly, suppose that the classical phase space consists of one regular and one chaotic region, with each wave function uniformly distributed over one of the two regions. Projecting these regions onto position space, let $f(\mathbf{r})$ be the fraction of the energy hypersurface at $\mathbf{r}$ that is part of the regular region, i.e., the fraction of momentum directions at $\mathbf{r}$ that correspond to stable trajectories. Then the average regular wave function has intensity $\overline{|\psi_{\mathrm{reg}}(\mathbf{r})|^2} = V^{-1} f(\mathbf{r})/\overline{f}$ at position $\mathbf{r}$, while the average chaotic wave function has intensity $\overline{|\psi_{\mathrm{ch}}(\mathbf{r})|^2} = V^{-1}(1 - f(\mathbf{r}))/(1 - \overline{f})$. Here $\overline{f} = \frac{1}{V}\int_V d\mathbf{r_a}\, f(\mathbf{r_a})$ is the total fraction of regular points in classical phase space, or equivalently the fraction of regular quantum eigenstates in the large kL limit. Then, starting with the expression (2) for the two-body matrix element we find that on average

$$v_{\alpha\beta} = \Delta V \int_V d\mathbf{r}\, \frac{1}{V^2}\frac{f^2(\mathbf{r})}{\overline{f}^2} = \Delta \frac{\overline{f^2}}{\overline{f}^2}, \tag{23}$$

whenever α and β are both regular states, to be compared with the overall average $\overline{v_{\alpha\beta}} = \Delta$ for *all* states α, β. Clearly, $v_{\alpha\beta}$ is enhanced by a factor of order unity, since the two regular states tend to be concentrated in the same region of

phase space. Similarly, by replacing f with $1-f$, we obtain enhanced $v_{\alpha\beta} = \Delta(\overline{f^2} - 2\overline{f} + 1)/(1-\overline{f})^2$ when both α and β are chaotic, and finally, below average interaction-matrix elements $v_{\alpha\beta} = \Delta(\overline{f^2} - \overline{f})/(\overline{f}^2 - \overline{f})$ are typically obtained when one single-particle state is regular and the other chaotic. Combining these results, we obtain the lower bound

$$\overline{\delta v_{\alpha\beta}^2} \geqslant \Delta^2 \left(\frac{\overline{f^2} - \overline{f}^2}{\overline{f} - \overline{f}^2} \right)^2, \tag{24}$$

where the quantity in parentheses is a classical system property independent of kL. Unless the local regular fraction $f(\mathbf{r})$ is a position-independent constant, this quantity is nonzero, and the standard deviation is necessarily of the order of Δ, i.e., of the same order as the average $v_{\alpha\beta}$. We note that Eq. (24) is a lower bound only, as it assumes that each regular or chaotic state is uniformly spread over its corresponding phase space region. Any intensity fluctuations within the set of regular states or within the set of chaotic states will only add to the total matrix element variance.

The kL independence of the variance for regular systems can also be inferred from the following simple argument: Regular-like quantum behavior is obtained when the ergodic time λ_*^{-1} of a chaotic system becomes of the same order as the Heisenberg time $\pi k L T_B$ needed to resolve the spectrum. Then the Thouless conductance $g_T \sim kL\lambda_* T_B$ is of order unity and Eqs. (14) and (17) obtained originally for chaotic dynamics imply $\overline{\delta v_{\alpha\beta}^2} \sim \Delta^2$. Thus, in both the chaotic and the regular (or mixed) situations, increased interaction-matrix element fluctuations can be understood as arising from excess wave-function localization, beyond what is expected from a random wave model.

The constant factor in Eq. (24) depends not only on the regular fraction $\overline{f}$ in phase space, but equally importantly on the relative size $\sim \overline{f}^2/\overline{f^2}$ of the position-space region in which the regular states live (i.e., the participation ratio of the regular states). For example, in the extreme case where all regular states live in in area $V_{\rm reg}$ and all chaotic states live in the complementary area $V - V_{\rm reg}$, we have $\overline{f} = \overline{f^2} = V_{\rm reg}/V$, and $\overline{\delta v_{\alpha\beta}^2} = \Delta^2$, independent of the size of $V_{\rm reg}$.

Equation (24) predicts very large enhancement, scaling as $(kL)^2/\ln kL$, of the matrix element variance in mixed dynamical systems, over the random-wave prediction. Large matrix element fluctuations in the presence of soft chaos have previously been observed in Ref. 32.

The diagonal matrix element variance $\overline{\delta v_{\alpha\beta}^2}$ is computed as a function of kL for two typical mixed phase-space quarter-lemon billiards and shown by dashed lines in Fig. 10. As expected, no falloff with kL is observed. In Fig. 11, we see that enhancement of an order of magnitude or more over random-wave behavior can easily be obtained for physically interesting values of kL. The most dramatic enhancement is observed for the $a = -0.25$ quarter-lemon billiard, which is closer to integrability.

Behavior intermediate between hard chaos and mixed chaotic and/or regular phase space is obtained in the presence of families of marginally stable classical trajectories, such as the "bouncing ball" orbits of the stadium billiard. In the quarter-stadium billiard ($s = 0$ in Fig. 1), exceptional states

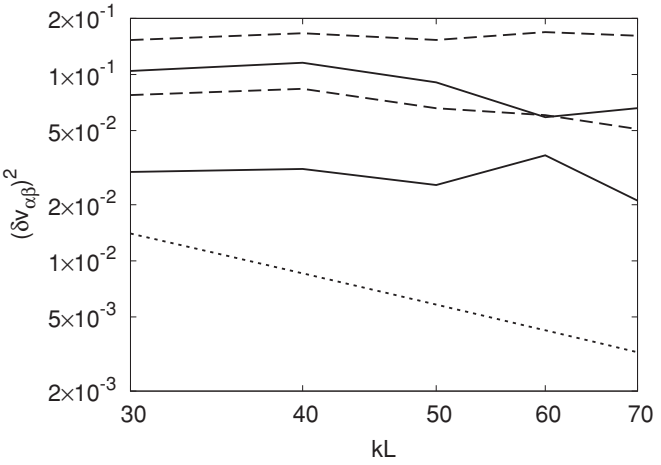

FIG. 10. The variance of $v_{\alpha\beta}$ for $a = 0.25, 1.00$ quarter-stadium billiards (upper and lower solid lines); $a = -0.25, -0.50$ quarter-lemon billiards (upper and lower dashed lines); random waves (dotted line). Neumann boundary conditions are used for all four billiards.

associated with such orbits are concentrated in the rectangular region of the billiard and constitute a fraction $\sim 1/(kL)^{1/2}$ of the total set of states.[41] When α and β are both bouncing-ball states, $\delta v_{\alpha\beta} = v_{\alpha\beta} - \overline{v_{\alpha\beta}} \sim \Delta$, just as would be the case for regular states concentrated in a finite fraction of the available coordinate space. These special matrix elements dominate the variance, leading to

$$\overline{\delta v_{\alpha\beta}^2} \sim \frac{\Delta^2}{kL}, \tag{25}$$

and implying an enhancement factor $\sim kL/\ln kL$ over the random-wave prediction. Numerical data for quarter-stadium billiards is shown by solid lines in Figs. 10 and 11. The stronger fluctuations are observed in the less chaotic $a = 0.25$ stadium.

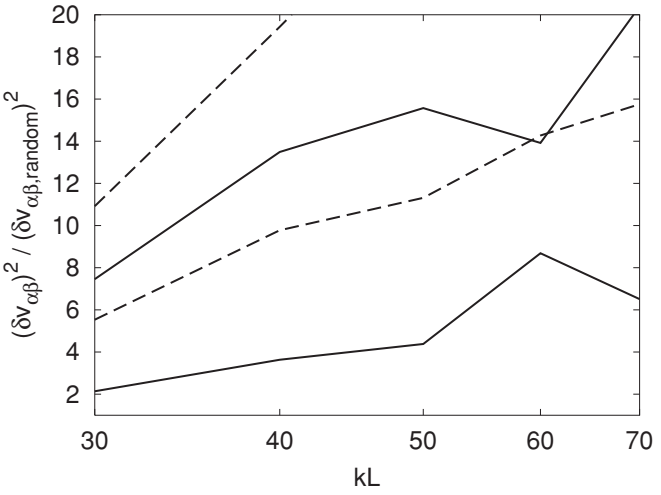

FIG. 11. Enhancement of the $v_{\alpha\beta}$ variance as compared with the random-wave prediction for $a = 0.25, 1.00$ quarter-stadium billiards (solid lines); $a = -0.25, -0.50$ quarter-lemon billiards (dashed lines). See Fig. 10.

2. *Fluctuation of $v_{\alpha\alpha}$ and $v_{\alpha\beta\gamma\delta}$*

A calculation analogous to the one resulting in Eq. (24) shows that $\overline{\delta v_{\alpha\alpha}^2}$ must also be $O(\Delta^2)$ and kL independent for a billiard with mixed phase space. In addition, the average $\overline{v_{\alpha\alpha}}$ is enhanced by an $O(1)$ factor from its random-wave value of 3Δ ($\beta = 1$) or 2Δ ($\beta = 2$). In the stadium billiard, the absence of a stable phase space region ensures that bouncing-ball states, with $\delta v_{\alpha\alpha} \sim \Delta$ and frequency $\sim 1/(kL)^{1/2}$ should dominate the double-diagonal matrix element variance:

$$\overline{\delta v_{\alpha\alpha}^2} \sim \frac{\Delta^2}{(kL)^{1/2}}. \tag{26}$$

The billiard results (not shown) are qualitatively consistent with the above predictions, although statistical noise prevents us from extracting a meaningful power-law behavior.

In contrast, fluctuations in the off-diagonal matrix elements $v_{\alpha\beta\gamma\delta}$ are relatively little affected by bouncing-ball orbits or even regular phase space regions. This is due to the fact that these elements are zero on average, not $O(\Delta)$, and thus an increase by an $O(1)$ factor of some matrix elements does not necessarily lead to a large variance. We may consider an extreme scenario where each eigenstate is located in one of two disjoint regions of area $V/2$. Clearly $v_{\alpha\beta\gamma\delta}$ is nonvanishing only when all four states are located in the same half of the billiard. In such a case, the typical $v_{\alpha\beta\gamma\delta}^2$ is enhanced by a factor of 8 compared with the random-wave prediction, ignoring logarithms. Because $1/8$ of all matrix elements $v_{\alpha\beta\gamma\delta}$ are nonzero, the variance $\overline{\delta v_{\alpha\beta\gamma\delta}^2}$ is nearly unchanged from the ergodic case. The above argument generalizes trivially to an arbitrary number of wave-function classes. Numerical data in quarter-stadium and quarter-lemon billiards (not shown) confirm that $\overline{\delta v_{\alpha\beta\gamma\delta}^2}$ is nearly independent of the classical dynamics in the billiard. Higher moments of the $\delta v_{\alpha\beta\gamma\delta}$ distribution are greatly enhanced in systems with mixed phase space, and the distribution becomes strongly non-Gaussian.

B. One-body matrix elements

In a billiard with mixed classical phase space, we expect the one-body matrix element v_α of the surface charge potential $\mathcal{V}$ to average $\int_V d\mathbf{r}\, \mathcal{V}(\mathbf{r}) f(\mathbf{r}) / \int_V d\mathbf{r}\, f(\mathbf{r}) = \overline{\mathcal{V}f}/\overline{f}$ for regular states, where $f(\mathbf{r})$ is the function defined in Sec. VI A 1, and similarly to average $(\overline{\mathcal{V}} - \overline{\mathcal{V}f})/(1 - \overline{f})$ for chaotic states. We then obtain a lower bound for the variance analogous to Eq. (24),

$$\overline{\delta v_\alpha^2} \geqslant \frac{(\overline{\mathcal{V}f} - \overline{\mathcal{V}}\,\overline{f})^2}{\overline{f} - \overline{f}^2}, \tag{27}$$

which is $O(\Delta^2)$ and independent of kL. Thus, Eq. (27) implies an enhancement by a factor $\sim kL$ over the variance for fully chaotic billiards given by Eq. (22). The absence of a falloff in the variance with increasing kL is consistent with our results for quarter-lemon billiards (dashed lines) in Fig. 12.

In the quarter-stadium billiard, bouncing-ball states with $\delta v_\alpha \sim \Delta$ will once again dominate the variance

$$\overline{\delta v_\alpha^2} \sim \frac{\Delta^2}{(kL)^{1/2}}, \tag{28}$$

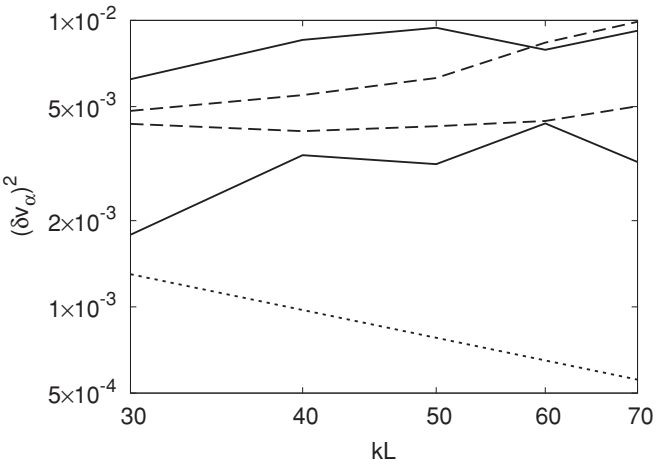

FIG. 12. The variance of v_α for $a = 0.25$, 1.00 quarter-stadium billiards (solid lines); $a = -0.25$, -0.50 lemon billiards (dashed lines); random waves (dotted line). Neumann boundary conditions are used for all four billiards.

which is a factor $\sim (kL)^{1/2}$ enhancement over random-wave behavior. The decay predicted by Eq. (28) is not observed in the numerical data in the experimentally relevant range $30 \leqslant kL \leqslant 70$ (solid lines in Fig. 12), suggesting once again that the energies are not high enough for the asymptotic large-kL scaling laws to be applicable. We do find that enhancement by a factor of 5 to 15 of the one-body matrix element variance is quite possible in the energy range of interest, when the billiard under consideration exhibits either soft chaos or marginally stable orbits in the classical dynamics.

VII. SUMMARY AND CONCLUSION

We have studied fluctuations of two-body and one-body matrix elements in chaotic billiards as a function of a semiclassical parameter kL, and compared them with the normalized random wave model predictions. Understanding the quantitative behavior of these fluctuations is important for the proper analysis of peak spacing statistics in the Coulomb blockade regime of weakly coupled chaotic quantum dots.

Dynamical effects, associated with nonrandom short-time behavior in actual chaotic systems, are formally subleading for two-body matrix elements, and of the same order as the random-wave prediction for one-body matrix elements. In practice, however, we find that these effects can easily lead to enhancement by a factor of 3 or 4 of the variance in both one-body and two-body matrix elements for experimentally relevant values of kL and in reasonable hard chaotic geometries. Somewhat larger enhancement factors are expected when time-reversal symmetry is broken by a magnetic field. The size of these dynamical corrections scales in each case as a power of λ_*^{-1}, a time scale associated with approach to ergodicity in the associated classical dynamics. Random-wave behavior is recovered in the limit $\lambda_*^{-1} \to 0$. In typical geometries, dynamical effects on matrix element fluctuations cannot be properly computed in a semiclassical approximation, as higher-order terms are quantitatively of the same size as the semiclassical expression in the kL range of

experimental interest. We have used a quantum map model to investigate the approach to semiclassical scaling at very large values of kL as well as the saturation of matrix element fluctuations at moderate to small values of kL.

In the case of the interaction-matrix element covariance for energy levels that are separated by less than the ballistic Thouless energy, dynamical effects are not only often larger than random-wave effects, but are also of opposite sign, leading to an overall covariance that is positive. This is in contrast with the random-wave model where the covariance is always negative. Nevertheless, the sum rule (19) is preserved due to large negative covariances for more widely separated states. We have discussed an analogy with similar behavior in diffusive systems.

Systems with a mixed chaotic-regular phase space or with families of marginally stable classical orbits show even stronger enhancement of matrix element fluctuations as compared with the random-wave model. We discussed the expected asymptotic scaling with kL of the matrix element fluctuations in these cases, and found it to be very different from the scaling found in chaotic systems.

Our results strongly indicate that wave function statistics in actual chaotic single-particle systems, including dynamical effects, are needed to make a proper quantitative comparison between theory (e.g., Hartree-Fock) and experiment. A better understanding of single-particle wave-function correlations is then essential for the calculation of observables in an interacting many-electron system, such as the peak spacing distribution in the Coulomb blockade regime of a quantum dot. Furthermore, these correlations need to be understood beyond the naive leading-order semiclassical approximation, to allow comparison with experiments, which are generally performed at moderate values of the semiclassical parameter kL.

ACKNOWLEDGMENTS

We acknowledge useful discussions with Y. Gefen, Ph. Jacquod, and C. H. Lewenkopf. This work was supported in part by the US Department of Energy Grants No. DE-FG03-00ER41132 and No. DE-FG-0291-ER-40608 and by the National Science Foundation under Grant No. PHY-0545390. We are grateful for the hospitality of the Institute for Nuclear Theory at the University of Washington, where this work was completed.

APPENDIX: QUANTUM MAP MODEL

To understand better the anomalously slow decay of $\overline{\delta v_{\alpha\beta}^2}$ and other matrix element fluctuations in realistic chaotic systems, we may consider a toy model (perturbed cat map[42]) that displays very similar behavior and for which it is easy to collect good statistics at very large values of kL. Define a classical map on the torus $(q,p) \in [-\pi,\pi) \times [-\pi,\pi)$ by

$$\begin{aligned} q_{t+1} &= q_t + K'(p_t) \bmod 2\pi, \\ p_{t+1} &= p_t - V'(q_{t+1}) \bmod 2\pi. \end{aligned} \tag{A1}$$

The above map may be obtained by stroboscopically viewing the periodically kicked Hamiltonian system

$$H(q,p,t) = K(p) + \sum_{n=-\infty}^{\infty} \delta(t-n)V(q). \tag{A2}$$

We choose the kick potential to be a perturbation of an inverted harmonic oscillator

$$\begin{aligned} V(q) = -\frac{q^2}{2} - A\cos q - B(4\cos q - \cos 2q) \\ + C(2\sin q - \sin 2q), \end{aligned} \tag{A3}$$

while the kinetic term governing free evolution between kicks is

$$K(p) = \frac{p^2}{2} + A\cos p + B(4\cos p - \cos 2p). \tag{A4}$$

$K(p)$ is even in p to preserve a time-reversal invariance (symmetry class $\beta = 1$). $V(q)$ and $K(p)$ have been chosen so that the map has a period-1 orbit at $q = p = 0$, with stability exponent

$$\lambda_0 = \cosh^{-1}\left[1 + \tfrac{1}{2}(1-A)^2\right] \approx 1 - A, \tag{A5}$$

where the approximate form holds for $\lambda_0 \ll 1$. Thus, A may be varied to change the stability of the shortest orbit, whereas the perturbations B and C, which have no effect on the linearized behavior around $q = p = 0$, allow for ensemble averaging while keeping the monodromy matrix of the central orbit fixed.

This map may be quantized using standard techniques;[37] the position basis is discrete with spacing $\hbar$ due to periodicity in momentum. The Hilbert space dimension, $N = 2\pi/\hbar$, plays the role of the semiclassical parameter $kL = pL/\hbar$ in the billiard system. The double integral of Eq. (3) must be replaced by a double sum

$$S = N^2 \sum_{\substack{i,j=1 \\ i\neq j}}^{N} [\overline{|\psi_i|^2|\psi_j|^2} - c]^2, \tag{A6}$$

where c is a constant that ensures

$$N^2 \sum_{\substack{i,j=1 \\ i\neq j}}^{N} [\overline{|\psi_i|^2|\psi_j|^2} - c] = 0. \tag{A7}$$

Note that since we are working in one dimension, we must drop the $i = j$ terms to prevent them from dominating the sum. Our one-dimensional toy model will not reproduce the $\ln kL/(kL)^2$ behavior that is associated with the short-distance $1/k \ll |\mathbf{r} - \mathbf{r}'| \ll L$ divergence of the 2D correlator. Instead, we can think of S as the analog of the 2D integral (3) with the short-distance part subtracted:

$$V^2 \int_V \int_V d\mathbf{r}\, d\mathbf{r}'\, C^2(\mathbf{r},\mathbf{r}') - \frac{3}{\pi}\left(\frac{2}{\beta}\right)^2 \frac{\ln kL}{(kL)^2} \sim \frac{b_g}{(kL)^2} + \cdots. \tag{A8}$$

Numerical results for the map are shown in Fig. 4. We observe the expected $S = b_{\mathrm{map}}/N^2$ semiclassical behavior for

large N, and the increase of the prefactor $b_{\rm map}$ with decreasing classical stability exponent λ_0 (see the discussion in Sec. III A). Furthermore, we note that even for the "typical" case $\lambda_0 = 1$, strong deviations from the simple power-law behavior appear for $N \leqslant 50$; even larger values of N are necessary to observe the correct power law for smaller λ_0. All the curves saturate at $S \approx 0.045$, leading to the appearance of a slower than $1/N^2$ decay at moderate N values. Thus, it is not surprising that a weaker than expected dependence on kL is observed for moderate kL values in Sec. III A.

As noted in Ref. 24, the interaction-matrix element covariance is suppressed relative to the variance by a factor $\sim kL$ or N, and the covariance is not a self-averaging quantity. To improve the poor ratio of signal to statistical noise, we may work with a larger ensemble defined by

$$V(q) = -\frac{q^2}{2} - A\cos q + V_{\rm rnd}(q)\Theta(|q| - q_0) \qquad \text{(A9)}$$

and

$$K(p) = \frac{p^2}{2} + A\cos p + K_{\rm rnd}(p)\Theta(|q| - p_0), \qquad \text{(A10)}$$

where $V_{\rm rnd}(q)$ and $K_{\rm rnd}(p)$ are random functions, $K_{\rm rnd}(p)$ is even to preserve time-reversal symmetry, and Θ is the step function: $\Theta(x) = 1$ for $x \geqslant 0$ and 0 otherwise. The local dynamics near the periodic orbit at $q = p = 0$ is unaffected by the ensemble of perturbations. In Fig. 5, we use $A = 0$ and $q_0 = p_0 = \pi/2$, but very similar behavior is obtained for other values of the parameters.

[1] T. Guhr, A. Müller-Groeling, and H. A. Weidenmüller, Phys. Rep. **299**, 190 (1998).
[2] Y. Alhassid, Rev. Mod. Phys. **72**, 895 (2000).
[3] D. Ullmo, Rep. Prog. Phys. **71**, 026001 (2008).
[4] I. L. Kurland, I. L. Aleiner, and B. L. Altshuler, Phys. Rev. B **62**, 14886 (2000).
[5] I. L. Aleiner, P. W. Brouwer, and L. I. Glazman, Phys. Rep. **358**, 309 (2002).
[6] R. A. Jalabert, A. D. Stone, and Y. Alhassid, Phys. Rev. Lett. **68**, 3468 (1992).
[7] Y. Alhassid and H. Attias, Phys. Rev. Lett. **76**, 1711 (1996).
[8] Y. Alhassid, Phys. Rev. B **58**, R13383 (1998).
[9] J. A. Folk, S. R. Patel, S. F. Godijn, A. G. Huibers, S. M. Cronenwett, C. M. Marcus, K. Campman, and A. C. Gossard, Phys. Rev. Lett. **76**, 1699 (1996).
[10] A. M. Chang, H. U. Baranger, L. N. Pfeiffer, K. W. West, and T. Y. Chang, Phys. Rev. Lett. **76**, 1695 (1996).
[11] J. A. Folk, C. M. Marcus, and J. S. Harris Jr., Phys. Rev. Lett. **87**, 206802 (2001).
[12] S. R. Patel, S. M. Cronenwett, D. R. Stewart, A. G. Huibers, C. M. Marcus, C. I. Duruöz, J. S. Harris Jr., K. Campman, and A. C. Gossard, Phys. Rev. Lett. **80**, 4522 (1998).
[13] S. R. Patel, D. R. Stewart, C. M. Marcus, M. Gökçedağ, Y. Alhassid, A. D. Stone, C. I. Duruöz, and J. S. Harris Jr., Phys. Rev. Lett. **81**, 5900 (1998).
[14] Y. Alhassid and T. Rupp, Phys. Rev. Lett. **91**, 056801 (2003).
[15] G. Usaj and H. U. Baranger, Phys. Rev. B **67**, 121308(R) (2003).
[16] U. Sivan, R. Berkovits, Y. Aloni, O. Prus, A. Auerbach, and G. Ben-Yoseph, Phys. Rev. Lett. **77**, 1123 (1996).
[17] F. Simmel, T. Heinzel, and D. A. Wharam, Europhys. Lett. **38**, 123 (1997).
[18] S. Lüscher, T. Heinzel, K. Ensslin, W. Wegscheider, and M. Bichler, Phys. Rev. Lett. **86**, 2118 (2001).
[19] Y. Alhassid and S. Malhotra, Phys. Rev. B **66**, 245313 (2002).
[20] Ya. M. Blanter, A. D. Mirlin, and B. A. Muzykantskii, Phys. Rev. Lett. **78**, 2449 (1997).
[21] A. D. Mirlin, Phys. Rep. **326**, 259 (2000).
[22] Y. Alhassid and Y. Gefen, e-print arXiv:cond-mat/0101461.
[23] Y. Alhassid, H. A. Weidenmüller, and A. Wobst, Phys. Rev. B **76**, 193110 (2007).
[24] L. Kaplan and Y. Alhassid, Phys. Rev. B **78**, 085305 (2008).
[25] S. Tomsovic, D. Ullmo, and A. Bäcker, Phys. Rev. Lett. **100**, 164101 (2008); D. Ullmo, S. Tomsovic, and A. Bäcker, Phys. Rev. E **79**, 056217 (2009).
[26] J. D. Urbina and K. Richter, J. Phys. A **36**, L495 (2003).
[27] J. D. Urbina and K. Richter, Eur. Phys. J. Special Topics **145**, 255 (2007).
[28] L. A. Bunimovich, Commun. Math. Phys. **65**, 295 (1979).
[29] R. Artuso and A. Prampolini, Phys. Lett. A **246**, 407 (1998); R. Artuso, Physica D **131**, 68 (1999).
[30] E. J. Heller, in *Chaos and Quantum Physics*, 1989 NATO Les Houches Summer School, edited by M. J. Giannoni, A. Voros, and J. Zinn-Justin (Elsevier, Amsterdam, 1991).
[31] B. L. Altshuler, Y. Gefen, A. Kamenev, and L. S. Levitov, Phys. Rev. Lett. **78**, 2803 (1997).
[32] D. Ullmo, T. Nagano, and S. Tomsovic, Phys. Rev. Lett. **90**, 176801 (2003); **91**, 179901(E) (2003).
[33] S. Hortikar and M. Srednicki, Phys. Rev. Lett. **80**, 1646 (1998).
[34] J. D. Urbina and K. Richter, Phys. Rev. E **70**, 015201(R) (2004).
[35] M. C. Gutzwiller, *Chaos in Classical and Quantum Mechanics* (Springer, New York, 1990).
[36] I. V. Gornyi and A. D. Mirlin, Phys. Rev. E **65**, 025202(R) (2002); J. Low Temp. Phys. **126**, 1339 (2002).
[37] S. Fishman, D. R. Grempel, and R. E. Prange, Phys. Rev. Lett. **49**, 509 (1982).
[38] A. Altland and M. R. Zirnbauer, Phys. Rev. Lett. **77**, 4536 (1996).
[39] E. J. Heller, Phys. Rev. Lett. **53**, 1515 (1984).
[40] A. Ossipov, T. Kottos, and T. Geisel, Phys. Rev. E **65**, 055209(R) (2002).
[41] A. Bäcker, R. Schubert, and P. Stifter, J. Phys. A **30**, 6783 (1997).
[42] P. A. Boasman and J. P. Keating, Proc. R. Soc. London, Ser. A **449**, 629 (1995).